Numerical Analysis and Precursor Detonation Tube Design for Continuously Rotating Detonation Engine Development

Johaneev Sheelam[1] and Krish Sharma.[2]

Embry-Riddle Aeronautical University, Prescott, Arizona, 86301, USA

Kyle C. Mooney[3]

Embry-Riddle Aeronautical University, Prescott, Arizona, 86301, USA

Bali J. Coulter[4]

Embry-Riddle Aeronautical University, Prescott, Arizona, 86301, USA

Conventional chemical rocket engines are fundamentally limited by deflagration-based combustion, which constrains pressure rise and overall thermodynamic efficiency. Detonation-based combustion offers a pressure-gain alternative, but practical implementation—particularly in rotating detonation engines (RDEs)—is challenged by ignition control, stability, deflagration-to-detonation transition (DDT), and diagnostic limitations. This study supports ongoing rotating detonation engine development at Embry-Riddle Aeronautical University through a risk-reduction investigation using a linear detonation tube as a simplified, system-adjacent experimental platform. Three-dimensional ANSYS CFX simulations were used to assess confinement behavior and transient pressure evolution within the detonation tube and CRDE geometries. A revised CFX configuration that suppressed secondary wave interference produced a single dominant wave structure, yielding pressure magnitudes in close agreement with the reduced-order MATLAB solver. Results indicate that the proposed detonation tube configuration can support conditions consistent with early-stage DDT while maintaining feasible structural and diagnostic limits, and that the CRDE chamber and exhaust geometries can sustain confined detonation behavior with effective exhaust expansion at the system level. Although experimental validation remains forthcoming, the analyses provide quantitative justification for fabrication and staged testing, supporting progression toward integrated detonation-based propulsion development.

I. Nomenclature

a = Speed of sound	r_o = Outer radius of tube	α = Pressure detection multiplier
B = Burnedness metric	S_L = Left Riemann signal speed	β = Burnedness parameter
c = Local acoustic speed	S_R = Right Riemann signal speed	β = Burnedness detection threshold
c_p = Specific heat at constant pressure	S_{allow} = Allowable stress	γ = Ratio of specific heats
c_v = Specific heat at constant volume	S_u = Ultimate tensile strength	Δp = Gauge pressure
D = Detonation wave speed	S_y = Yield strength	Δt = Time step
D_{CJ} = Chapman-Jouguet detonation velocity	T = temperature	Δx = Spatial grid spacing
E = Total specific energy	T_0 = Initial temperature	ρ = Density

[1] B.S Student, Aerospace + Electrical Engineering, and AIAA Student Member.

[2] B.S Student, Aerospace Engineering and AIAA Student Member

[3] B.S Student, Aerospace Engineering, and AIAA Student Member

[4] B. S Student, Mechanical Engineering, and AIAA Student Member

F = Numerical flux vector
h = Specific enthalpy
J_k = Diffusive mass flux of species k
L_{DDT} = Run-up length
p = pressure
p_{amb} = Ambient pressure
r = Radial coordinate
r_i = Inner radius of tube
T_{th} = Temperature detection threshold
u = Velocity
U = Vector of conserved variables
W_k = Molecular weight of species k
x = Axial coordinate
Y_k = Mass fraction of species k
Y_f = Fuel mass fraction
$Y_{f,0}$ = Initial fuel mass fraction
σ_r = Radial stress
σ_θ = Hoop stress
σ_z = Axial stress
σ_{vm} = von Mises equivalent stress
τ = Viscous stress tensor
$\dot{\omega}_k$ = Species production rate
$\dot{\omega}_T$ = Volumetric heat release rate

II. Introduction

Detonation-based combustion represents a fundamentally different heat-release regime in which chemical energy release is coupled to a supersonic shock front, producing rapid pressure rise across the reaction zone. Classical detonation theory, including the Chapman–Jouguet (CJ) condition [1] and the Zel'dovich–von Neumann–Döring (ZND) model [2], describes a self-sustaining shock-induced reaction structure governed by conservation of mass, momentum, and energy. These relationships form the theoretical basis for pressure-gain combustion and modern detonation engine research.

Propulsion applications of detonation have been investigated for decades, beginning with pulse detonation engine (PDE) concepts [3]. More recently, the continuously rotating detonation engine (CRDE) has emerged as a configuration capable of sustaining quasi-steady detonation wave propagation within an annular chamber. Unlike PDE architectures, CRDEs enable continuous pressure-gain combustion with reduced valving complexity and improved thrust density [4]. While experimental and numerical studies have demonstrated feasibility, challenges remain in ignition control, wave stability, confinement behavior, and structural survivability.

The present study adopts a modeling-centered approach to early-stage CRDE development. The broader research objective is a liquid oxygen (LOX) and kerosene CRDE suitable for first-stage thrust; however, this work focuses on development of a numerical framework and linear detonation tube precursor for risk reduction and feasibility bounding. A 1:3 ethylene–oxygen (C_2H_4/O_2) mixture is employed as a laboratory surrogate due to its well-characterized CJ properties and established detonation behavior [5].

Three-dimensional CFD simulations and a reduced one-dimensional reactive flow solver are used to estimate detonation velocity bounds, transient pressure magnitudes, confinement behavior, and pressure-driven structural loading for both linear and annular geometries. The objective is not predictive validation of sustained rotating detonation, but the establishment of physically consistent feasibility bounds to inform geometry selection, structural margin assessment, and driver–driven pressure matching prior to hardware fabrication. In the present study, ANSYS CFX is used in a turbulence-modeling capacity to characterize turbulence levels and qualitative confinement trends; detonation-scale wave-speed and pressure bounds are obtained from the reduced-order MATLAB framework.

III. Theoretical Background

This section summarizes the governing relations and assumptions used to bound detonation-relevant wave speeds, pressure rise, and pressure-driven structural loading for a linear detonation tube precursor study supporting continuously rotating detonation engine (CRDE) development. The framework integrates (i) classical detonation theory (CJ/ZND) as a reference for feasibility bounding and interpretation, (ii) one-dimensional compressible flow (Euler equations and Riemann Transport Theory) to capture shock-like transients and wave propagation trends, (iii) finite-rate chemical kinetics advanced via a constant-volume per-cell approximation using Cantera, and (iv) thick-walled cylinder stress relations (Lamé theory) used to convert local transient pressure into inner-wall stress and von Mises equivalent stress.

The objective is not predictive validation of steady detonation operation, but rather the establishment of physically consistent order-of-magnitude bounds and diagnostic/structural feasibility metrics prior to hardware fabrication and staged experimental testing.

A. Detonation Theory Benchmarks

1. Chapman-Jouguet Condition and Jump Relations

Detonation is a shock-coupled combustion wave in which chemical energy release occurs on a time scale comparable to the hydrodynamic compression time scale. Classical detonation theory represents detonation as a discontinuity satisfying conservation of mass, momentum, and energy across the wave. In a wave-fixed frame, the Rankine–Hugoniot relations may be written as:

Mass:

$$\rho_0 D = \rho_1 (D - u_1) \tag{1}$$

Momentum:

$$p_1 - p_0 = \rho_0 D\, u_1 \tag{2}$$

Energy:

$$h_1 + \frac{(D - u_1)^2}{2} = h_0 + \frac{D^2}{2} \tag{3}$$

Where subscript *0* denotes the unburned (pre-wave) state, subscript 1 denotes the post-wave state, *D* is the wave speed relative to the laboratory frame, u_1 is post-wave particle velocity, and *h* is specific enthalpy. For the Chapman-Jouguet (CJ) detonation, the flow immediately behind the wave is sonic relative to the wave:

$$D - u_1 = a_1 \tag{4}$$

The CJ solution provides a widely used reference detonation velocity D_{CJ} and post-wave thermodynamic state for a given mixture and initial condition, which can be used to define expected detonation-scale wave speeds and pressure magnitudes against which numerical and experimental trends may be compared. [6]

2. ZND Structure and DDT Interpretation

The Zel'dovich–von Neumann–Döring (ZND) model describes detonation as a leading shock followed by an induction zone and a finite-rate reaction zone. While the present numerical framework does not attempt to resolve ZND length scales in detail, the ZND model provides a conceptual basis for interpreting ignition delay, flame acceleration, and rapid pressure rise during deflagration-to-detonation transition (DDT**).** [2]

3. Practical Detonability Metrics

In experimental detonation tubes and annular rotating detonation chambers, detonability depends not only on CJ properties but also on mixture sensitivity and geometry. Three common practical concepts are noted here for context. (i) detonation cell size λ: a mixture-dependent length scale describing transverse instability structures. Smaller λ generally indicates easier detonability and shorter DDT run-up lengths. (ii) DDT run-up length L_{DDT}: the distance required for a deflagration to accelerate and couple to a shock to form detonation; this depends on mixture, initial pressure/temperature, confinement, and turbulence generation. (iii) Critical diameter d_{crit}: a minimum tube diameter required for stable detonation propagation for a given mixture and initial state.

These concepts are referenced for interpretation and to motivate geometry selection; the present study focuses on bounding pressure and wave-speed environments rather than predicting L_{DDT}, λ, or d_{crit} directly [7].

B. Governing Conservation Equations in Conservative Form (ANSYS CFX)

The governing compressible Navier–Stokes and species conservation equations are solved in conservative form using ANSYS CFX [8], ensuring shock-capturing consistency with discontinuity jump relations [9].

C. One-Dimensional Compressible Flow Model (Reduced Form Used in MATLAB)

For the reduced-order detonation tube feasibility model developed in MATLAB, transverse gradients, viscosity, and diffusive transport are neglected. The governing equations reduce to the one-dimensional inviscid Euler equations written in conservative form:

$$\frac{\partial}{\partial t}\begin{bmatrix}\rho \\ \rho u \\ \rho E\end{bmatrix} + \frac{\partial}{\partial x}\begin{bmatrix}\rho u \\ \rho u^2 + \rho \\ u(\rho E + \rho)\end{bmatrix} = 0 \tag{9}$$

The total specific energy is defined as:

$$E = e + \frac{u^2}{2} \tag{10}$$

The finite-volume update used in the solver is:

$$\boldsymbol{U_i^{n+1}} = \boldsymbol{U_i^n} - \frac{\Delta t}{\Delta x}\left(\boldsymbol{F}_{i+\frac{1}{2}} - \boldsymbol{F}_{i-\frac{1}{2}}\right) \tag{11}$$

Left- and right-going wave speeds used for approximate Riemann flux evaluation are estimated from local primitive states:

$$S_L = \min(u_L - a_L, u_R - a_R), \qquad S_R = \max(u_L + a_L, u_R + a_R) \tag{12) (13}$$

The local sound speed is computed as:

$$a = \sqrt{\gamma \frac{p}{\rho}}, \qquad \gamma = \frac{c_p}{c_v} \tag{14}$$

The explicit time step is restricted by a CFL condition:

$$\Delta t = CFL \frac{\Delta x}{\max(|u_i| + a_i)} \tag{15}$$

This reduced model is used to obtain trend-bounding wave propagation and pressure evolution suitable for structural and diagnostic feasibility screening, rather than detailed viscous flame-structure prediction [9].

D. Thermochemistry and Finite-Rate Chemistry Coupling (Cantera)

Thermochemical properties and finite-rate chemical kinetics are obtained using Cantera [10] with a detailed gas-phase mechanism (GRI-Mech 3.0 in the present implementation). The gas is treated as calorically imperfect; c_p, c_v, and γ vary with temperature and species composition. Species mass fractions satisfy [11]:

$$\sum_k Y_k = 1 \tag{16}$$

1. Energy Consistency and State Recovery

The conserved total energy density is stored as:

$$\rho E = \rho(e + \frac{u^2}{2}) \tag{17}$$

The internal energy is recovered during the hydrodynamic update as:

$$e = \frac{E}{\rho} - \frac{u^2}{2} \tag{18}$$

The thermodynamic state is then recovered using Cantera from (ρ, e, Y), enabling calculation of $p, T, c_p, and\ c_v$ without assuming a constant γ.

2. Operator Splitting and Constant-Volume Chemistry

Chemical source terms are incorporated using an operator-split approach. After the Euler transport update, each cell is advanced as a constant-volume reactor for the same time step Δt. This constant volume approximation provides a practical coupling strategy for bounding rapid heat release and pressure rise in each cell; it does not attempt to resolve ZND induction-zone length scales or turbulence-driven flame acceleration physics [10].

E. Shock and Detonation/Reaction-Front Identification Marks/Methods

For diagnostic tracking, the numerical framework distinguishes between (i) shock-like compressive fronts and (ii) detonation-like strongly reacting zones using combined thresholds on pressure rise, temperature rise, and fuel consumption [12]. A detonation-like region is identified using:

$$p > \alpha p_{amb}, \qquad T > T_{th}, \qquad \beta > \beta_{th} \tag{19}$$

A "burnedness" metric is defined using fuel mass fraction Y_f:

$$B = 1 - \frac{Y_f}{Y_{f,0}} \tag{20}$$

This criterion reduces false positives in regions where an inert shock produces elevated pressure and temperature without substantial reaction progress. The detection metric is used for front tracking and stop conditions rather than as proof of a resolved detonation structure.

F. Pressure-Driven Structural Loading (Thick-Walled Cylinder/Lamé Theory)

Pressure-driven structural loading is bounded by mapping local transient internal pressure to inner-wall stress using thick-cylinder elastic relations. Gauge pressure is defined as:

$$\Delta p(x,t) = \max\left(p(x,t) - p_{amb}, 0\right) \tag{21}$$

For a thick-walled cylinder with inner radius r_i and outer radius r_o the principal stresses at the inner surface $r = r_i$ are [12]:

Radial Stress:

$$\sigma_r(r_i) = -\Delta p \tag{22}$$

Hoop (circumferential) stress (Lamé):

$$\sigma_\theta(r_i) = \Delta p \frac{r_0^2 + r_i^2}{r_0^2 - r_i^2} \tag{23}$$

Axial Stress (end-condition dependent):

$$\sigma_z = \begin{cases} \Delta p \dfrac{r_i^2}{r_0^2 - r_i^2}, open\ ends \\ 0 \end{cases} \tag{24}$$

An equivalent von Mises stress is computed from the principal stresses:

$$\sigma_{vm} = \sqrt{\frac{1}{2}\left[(\sigma_\theta - \sigma_z)^2 + (\sigma_z - \sigma_r)^2 + (\sigma_r - \sigma_\theta)^2\right]} \tag{25}$$

Material allowables are treated in a pressure-vessel style conservative form:

$$S_{allow} = \min\left(\frac{S_y}{1.5}, \frac{S_u}{3.5}\right) \tag{26}$$

Temperature knockdown factors are applied to $S_y$and $S_u$to provide a conservative screening tool for feasibility and diagnostic survivability under impulsive internal pressure loading.

G. Reflected/End-Wall Loading Context

Detonation tubes may experience amplification of local pressure due to wave reflection at closed boundaries [7]. An incident shock or detonation wave reflecting from a closed end can produce a reflected compression that increases peak pressures relative to the incident wave, affecting end-region structural loading and instrumentation survivability. While the present study primarily uses the numerically obtained transient pressure field to estimate stress, reflected-wave amplification is noted as an important risk contributor in practical testing and informs conservative structural and diagnostic margin selection.

IV.Numerical Framework and Modeling Methodology

This section describes the implementation of the numerical methods and frameworks presented above, used to evaluate detonation-relevant wave propagation, ignition behavior, and pressure driven structural loading in the linear detonation tube configuration. Two complementary modeling approaches were employed: (1) A reduced one-dimensional compressible flow solver with finite-rate chemistry developed in MATLAB, and (2), Three-dimensional compressible reactive flow simulations performed in ANSYS CFX to evaluate geometry-dependent pressure distribution trends and confinement behavior.

The objective of the numerical framework is not high-fidelity detonation structure resolution, but rather physically consistent bounding of wave speeds, pressure magnitudes, ignition-induced transients, and structural loading environments relevant to precursor CRDE development.

A. One-Dimensional Reactive Flow Solver Implementation

The one-dimensional solver was developed in MATLAB to capture axial wave propagation and ignition-driven pressure transients within the detonation tube. The solver advances the conservative variables

$$\boldsymbol{U} = \begin{bmatrix} \rho \\ \rho u \\ \rho E \end{bmatrix} \tag{27}$$

using an explicit finite-volume formulation.

The domain is discretized uniformly into N_x control volumes of width Δx, and time advancement is performed using a CFL-limited explicit scheme.

Boundary conditions are implemented as reflective (zero-gradient) conditions at domain ends to approximate closed-tube behavior during early-stage wave propagation.

1. Spatial Discretization and Flux Evaluation

Interface fluxes are computed using an approximate Riemann formulation in an HLLC-like structure. Signal speeds are estimated using local primitive states as defined in Section III.C.

The update equation applied at each time step is:

$$\boldsymbol{U_i^{n+1}} = \boldsymbol{U_i^n} - \frac{\Delta t}{\Delta x}\left(\boldsymbol{F}_{i+\frac{1}{2}} - \boldsymbol{F}_{i-\frac{1}{2}}\right) \tag{28}$$

An explicit CFL condition enforces stability based on the maximum local characteristic speed.

2. Initial Conditions and Tube Configuration

The tube is initialized using a single-section configuration with an ignition kernel placed 0.2 centimeters from $x = 0$, where the initial velocity is $u = 0$. The mixture used for the feasibility model is C_2H_4/O_2, with equivalence ratio $\phi = 1.2$, selected to represent a detonable hydrocarbon-oxygen system with well characterized detonation properties.

A localized ignition kernel is optionally imposed near the wall interface to seed rapid reaction and evaluate detonation-like wave formation behavior.

3. Finite-Rate Chemistry Coupling

After each hydrodynamic update, chemistry is advanced using a constant-volume IdealGasReactor in Cantera over the same time step. Energy consistency is maintained by updating total energy after chemistry advancement. This allows for (i) consistent thermodynamic closure, (ii) variable γ, (iii) temperature-dependent reaction rates, (iv) and proper energy release coupling.

4. Shock and Detonation Front Tracking

Front tracking is implemented by monitoring spatial pressure gradients and combined reaction metrics. A shock front is identified from local maxima in pressure gradient magnitude. A detonation-like region is identified using combined pressure, temperature, and burnedness thresholds defined in Section III.E.

Tracked quantities include (i) peak pressure magnitude, (ii) peak temperature, (iii) front position versus time, (iv) average front speed, (v) maximum von Mises stress, and (vi) time-to-yield and time-to-allowable exceedance. These metrics provide quantitative feasibility bounds prior to hardware fabrication.

B. Structural Evaluation Procedure

At each time step, the transient internal pressure field is mapped to inner-wall stresses using Lamé relations (Section III.F). The following quantities are computed: (i) radial stress, (ii) hoop stress, (iii) axial stress, and (iv) von Mises equivalent stress. Temperature-dependent material strength metrics are evaluated using tabulated knockdown factors. Nodes exceeding yield, allowable stress, or ultimate strength are logged, enabling first-event detection and structural screening. This procedure provides order-of-magnitude estimates of (i) yield onset time, (ii) allowable exceedance time, (iii), and potential UTS rupture indicators.

C. Three-Dimensional CFD Modeling (ANSYS CFX)

Three-dimensional simulations were performed in ANSYS CFX to evaluate confinement behavior, turbulence development, and transient pressure evolution within the detonation tube and CRDE geometries. The compressible Navier–Stokes equations described in Section III.B were solved using a density-based formulation with a k–ωturbulence closure.

Initial CFX pressure fields exhibited two interacting compressive structures, complicating direct comparison with the reduced-order MATLAB solver. To isolate the dominant propagating wave, the ignition kernel was repositioned closer to the driven-front interface, allowing the primary wave to rapidly envelop the secondary disturbance. This revised configuration produced a single dominant wave structure more consistent with the one-dimensional propagation assumed in the MATLAB framework.

In the present study, CFX serves two roles: (i) turbulence validation and multidimensional flow characterization relevant to flame acceleration and DDT, and (ii) corroboration of pressure-rise trends observed in the reduced-order solver. The MATLAB framework remains the primary tool for detonation-scale wave-speed and pressure bounding, while CFX provides geometric and turbulence context.

V. Results and Discussion

All simulations were performed at $\phi = 1.2$, $T_0 = 293K$, and $p_{amb} = 1{,}114{,}575\ Pa$. The detonation tube was modeled with closed-end boundary conditions over a 6 ft domain. Simulations were terminated as the primary right-running front approached the downstream boundary.

A. Global Pressure and Temperature Evolution

The global peak pressure and temperature histories are shown in Fig. 1 and Fig 2, respectively.

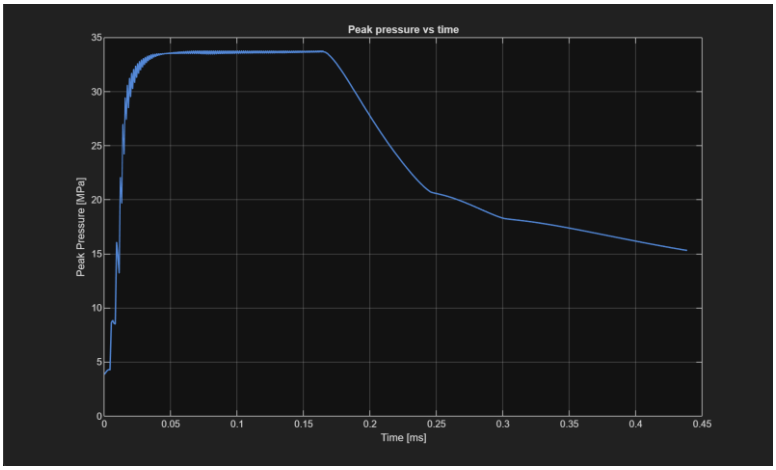

Fig. 1. Global peak pressure versus time for $\phi = 1.2$, closed-end configuration.

Peak pressure rises rapidly after ignition, reaching $p_{max} = 33.775\ MPa$ at $t = 0.163\ ms, and\ x = 1.75\ ft$. Early-time oscillations reflect ignition-driven compression and wave steepening. Beyond $0.16\ ms$, pressure decays due to expansion and redistribution within the confined domain.

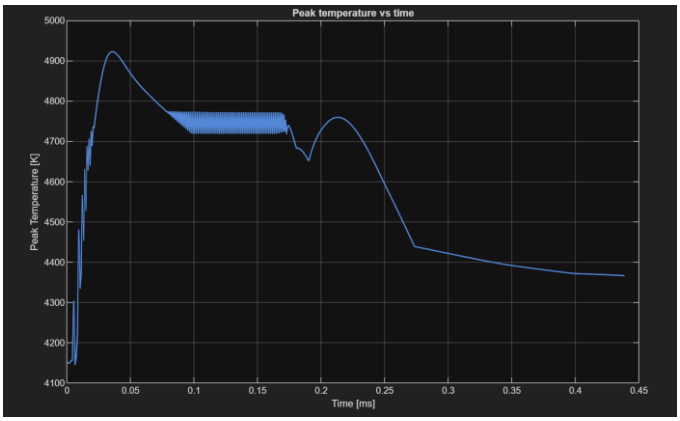

Fig. 2. Global peak wave temperature versus time.

The peak wave temperature reaches $T_{max} = 4923.1\ K$ at $t = 0.036\ ms$, and $0.10\ ft$. The earlier temperature peak relative to pressure is indicative of rapid local heat release prior to full pressure amplification along the tube length.

B. Front Propagation and Wave Speeds

Front tracking results are shown in Fig. 3.

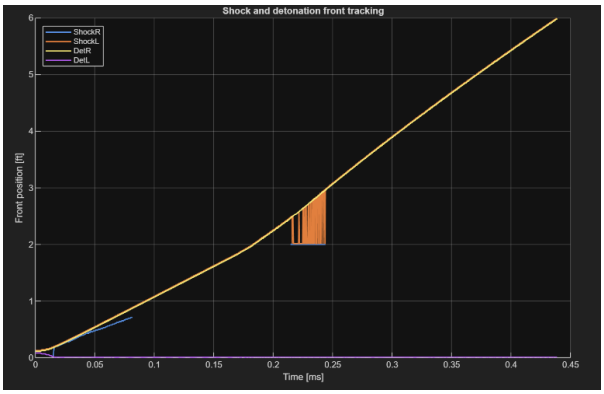

Fig. 3. Shock and detonation front position versus time.

The NaN-filtered front speeds, excluding the non-detonation paired fronts are:

- Shock (Left): 4454.6 m/s
- Detonation (Right): 4357.7 m/s

The left-running detonation speed is negligible, confirming primarily unidirectional propagation under the present ignition configuration. The tracking algorithm linked the left-running shock with the right-running detonation front, rather than pairing right-running shock and detonation fronts, explaining the apparent mismatch. The right-running detonation propagates at approximately $D_{num} = 4358 \frac{m}{s}$. For the present mixture ($\phi = 1.2, T_0 = 293K, p_0 = 1{,}114{,}575\ Pa$,) classical Chapman-Jouguet (CJ) theory predicts detonation velocities on the order of $D_{CJ} = 4300 - 4500 \frac{m}{s}$, depending on mechanism and thermodynamic closure assumptions.

The numerical result therefore lies within the expected CJ velocity band, with a relative deviation of less than approximately 2–3% from typical CJ predictions for comparable mixtures and initial states. This agreement indicates that the coupled Euler–finite-rate chemistry framework captures detonation-scale wave propagation consistent with classical theory, despite the use of a reduced one-dimensional representation and operator-split chemistry treatment.

C. Structural Response

Peak von Mises stress evolution is shown in Fig. 4.

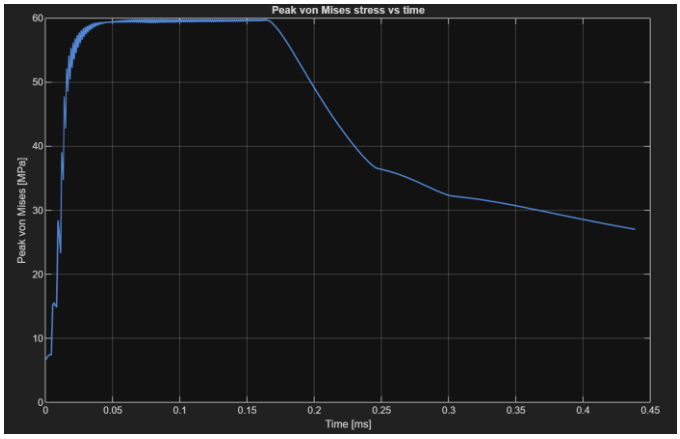

Fig. 4. Peak von Mises stress versus time.

The maximum computed equivalent stress was $\sigma_{vm,max} = 59.815\ MPa$ at $t = 0.163\ ms$, and $x = 1.75\ ft$. For the closed end configuration, axial stress contributions were included. The predicted stress remains well-below SS 304 material limits:

- $S_y = 240\ MPa$

- $S_u = 540\ MPa$

No yield, allowable exceedance, or UTS (Ultimate Failure Events) were recorded. Therefore, no structural violations were detected during the simulated interval.

D. Spatial Histories

Pressure, temperature, and von Mises stress histories at multiple axial locations are shown in Fig. 6.

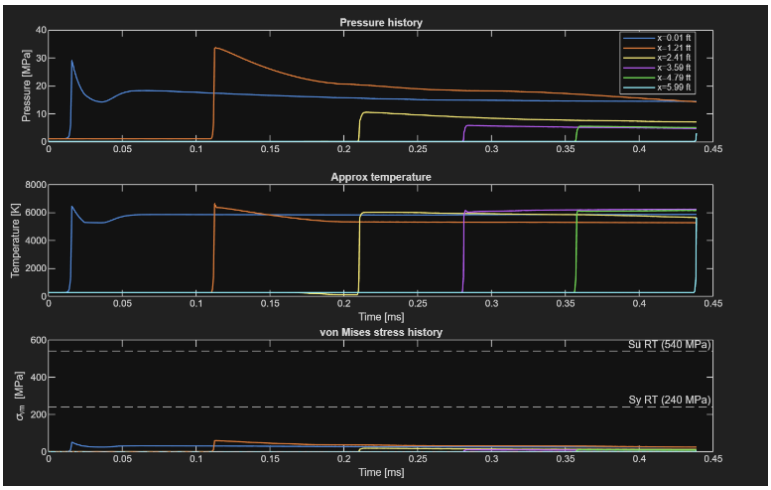

Fig. 5. Pressure, temperature, and stress histories at representative monitor points (nodes).

These traces illustrate wave steepening, peak compression near mid-domain, and gradual attenuation as expansion waves redistribute energy.

E. ANSYS CFD Results

Initial ANSYS CFX pressure fields revealed two interacting compressive structures, which complicated direct comparison with the reduced-order MATLAB solver. Because the transient solution contains both incident and reflected waves, detonation-scale pressure rise was interpreted from local pressure differentials relative to ambient conditions rather than from raw absolute pressure values.

Fig. 6 and Fig. 7 illustrate this behavior. The pressure-gradient field highlights the coexistence of a right-running detonation front and a secondary left-running compressive structure generated by boundary interaction during the early propagation phase. The pressure scale indicates that detonation-scale pressure rise was interpreted from local pressure differentials relative to ambient rather than from raw absolute pressure.

Fig. 6. Pressure-gradient field from the initial ANSYS CFX simulation showing two interacting compressive structures during early propagation. The right-running detonation front is displayed and a secondary left-running compressive wave generated by boundary interaction is displayed in Fig.10. $t = 0.69985$ ms.

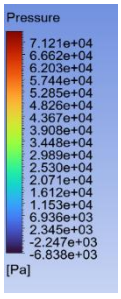

Fig. 7. Pressure-gradient scale corresponding to Fig. 6. Pressure rise is interpreted from local pressure differentials relative to ambient conditions to isolate detonation-scale compression in the presence of interacting waves.

To isolate the dominant wave and improve interpretability, the ignition kernel was repositioned closer to the closed-end boundary at $x = 0.01$ ft. This adjustment allowed the primary detonation front to rapidly envelop the secondary disturbance, effectively producing a near-unidirectional propagation regime. The resulting pressure field is shown in Fig. 8, with the corresponding pressure scale provided in Fig. 9. In this configuration, the dominant wave structure closely matches the propagation trend predicted by the MATLAB solver within 14%, enabling more direct comparison of axial pressure evolution.

Fig 8. Pressure gradient after moving ignition kernel, allowing for a near-instant unidirectional wave.

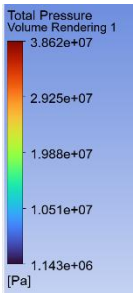

Fig. 9. Pressure gradient legend, showcasing corroboration with MATLAB

In addition to pressure evolution, the k–ω turbulence model resolves shear-layer formation and turbulence development surrounding the propagating wave. The resulting turbulent flow field (Fig. 10) and corresponding velocity scale (Fig. 11) provide insight into mixing behavior and confinement-driven flow features relevant to flame acceleration and deflagration-to-detonation transition (DDT).

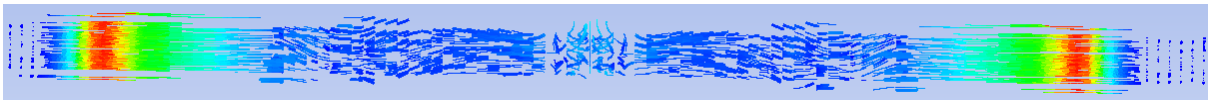

Fig. 10. Turbulence field resolved by the k–ω model in ANSYS CFX, illustrating shear-layer development and mixing surrounding the propagating detonation wave.

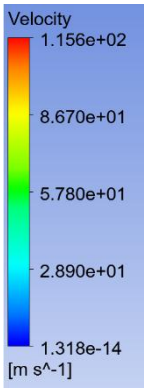

Fig. 11. Velocity magnitude scale corresponding to the turbulent flow field of the gas around the wave shown in Fig. 10.

VI. Conclusions and Future Work

This study presented a numerical modeling framework and precursor detonation tube design intended to support early-stage development of a continuously rotating detonation engine (CRDE). The objective was not predictive validation of steady rotating detonation operation, but rather the establishment of physically

consistent feasibility bounds for ignition behavior, detonation-scale wave propagation, and pressure-driven structural loading prior to hardware fabrication.

For the modeled configuration ($\phi = 1.2, T_0 = 293\ K, p_0 = 1{,}114{,}575\ Pa$), closed-end tube results demonstrate detonation-scale wave propagation consistent with CJ predictions and structural feasibility within conservative margins, indicating that the reduced-order numerical framework captures first-order detonation behavior consistent with classical theory, and structural integrity is maintained.

A. ANSYS Multidimensional Corroboration

Preliminary comparison indicates that the reduced-order solver captures the dominant pressure-rise magnitudes and wave-propagation trends observed in the revised ANSYS CFX simulations. While the three-dimensional CFD solution resolves turbulence and multidimensional confinement effects not represented in the one-dimensional framework, the revised single-wave configuration produces pressure magnitudes consistent with the MATLAB prediction. The CFX simulations therefore provide multidimensional corroboration of pressure evolution while simultaneously validating turbulence development relevant to flame acceleration and DDT.

B. Future Work

The modeling framework integrates classical CJ/ZND theory, one-dimensional compressible flow, finite-rate thermochemistry via Cantera, and thick-cylinder stress relations. Although viscous flame acceleration, turbulence-driven DDT physics, and azimuthal rotating detonation effects are beyond the present scope, the framework establishes quantitative bounds for experimental planning and system-level risk reduction.

Future work will focus on detonation tube fabrication and staged experimental validation of ignition behavior, flame acceleration, and pressure loading. Experimental data will be used to refine detection metrics, reconcile predicted and measured wave speeds and pressures, and improve hydrodynamic–chemistry coupling fidelity. The framework will subsequently be extended to rotating geometries in support of thrust-capable CRDE development.

References

[1] Jouguet, J. C., “Sur la Propagation des Réactions Chimiques dans les Gaz,” Journal de Mathématiques Pures et Appliquées, Series 6, Vol. 1, 1905, pp. 347–425 (extension of CJ theory).

[2] Zel’dovich, Ya. B., “On the Theory of the Propagation of Detonation in Gaseous Systems,” Zhurnal Éksperimental’noĭ i Teoreticheskoĭ Fiziki, Vol. 10, 1940 (English trans. NACA TM 1261, 1950); von Neumann, J., “Theory of Detonation Waves,” OSRD Report 549, 1942; and Döring, W., “Über Detonationsvorgang in Gasen,” Annalen der Physik, Vol. 43, 1943 (classical ZND detonation model).

[3] Nicholls, J. A., and Cullen, R. E., “The Feasibility of a Detonation Wave Rocket Motor,” Proceedings of the Seventh Symposium (International) on Combustion, The Combustion Institute, Pittsburgh, PA, 1959, pp. 514–527.

[4] Paxson, D. E., and Perkins, H. D., “A Simple Model for Rotating Detonation Rocket Engine Sizing and Performance Estimates,” AIAA Paper 2021-0192, AIAA SciTech Forum, 2021. https://doi.org/10.2514/6.2021-0192.

[5] Iyer, M. S. K., Ivin, K., and Singh, A. V., “Exploring Critical Detonation Parameters in Ethylene–Oxygen Detonations,” AIP Conference Proceedings, Vol. 2584, 2023, pp. 030019-1–030019-8. https://doi.org/10.1063/5.0127733

[6] Fickett, W., and Davis, W. C., *Detonation: Theory and Experiment*, Dover Publications, Mineola, NY, 2000.

[7] Lee, J. H. S., *The Detonation Phenomenon*, Cambridge University Press, Cambridge, England, 2010. https://doi.org/10.1017/CBO9780511754708.

[8] ANSYS, Inc., *ANSYS CFX-Solver Theory Guide*, Release 2023 R2, ANSYS, Inc., Canonsburg, PA, 2023.

[9] Toro, E. F., *Riemann Solvers and Numerical Methods for Fluid Dynamics: A Practical Introduction*, 3rd ed., Springer-Verlag, Berlin, 2009. https://doi.org/10.1007/b79761

[10] Goodwin, D. G., Speth, R. L., Moffat, H. K., and Weber, B. W., “Cantera: An Object-Oriented Software Toolkit for Chemical Kinetics, Thermodynamics, and Transport Processes,” Version 3.0.0, 2023, https://www.cantera.org

[11] Smith, G. P., Golden, D. M., Frenklach, M., Moriarty, N. W., Eiteneer, B., Goldenberg, M., Bowman, C. T., Hanson, R. K., Song, S., Gardiner, W. C., Lissianski, V. V., and Qin, Z., “GRI-Mech 3.0,” 1999, http://www.me.berkeley.edu/gri_mech/.

[12] Budynas, R. G., and Nisbett, J. K., *Roark’s Formulas for Stress and Strain*, 8th ed., McGraw–Hill Education, New York, 2012.